The subsurface carbonation potential of basaltic rocks from the Jizan region of Southwest Saudi Arabia

Eric H Oelkers, Serguey Arkadakskiy, Abdulkader M Afifi, Hussein Hoteit, Maximillian Richards, Jakub Fedorik, Antoine Delaunay, Jose Eduardo Torres, Zeyad T Ahmed, Noushad Kunnummal, et al.

The subsurface carbonation potential of basaltic rocks from the Jizan region of Southwest Saudi Arabia

Eric H. Oelkers[1*], Serguey Arkadakskiy[2], Abdulkader M. Afifi[3], Hussein Hoteit [3], Maximillian Richards[4], Jakub Fedorik[3], Antoine Delaunay[3], Jose Eduardo Torres[3], Zeyad T. Ahmed[2], Noushad Kunnummal[2], Sigurdur R. Gislason[5]

1 Géosciences Environnement Toulouse (GET), CNRS UMR 5563, 14 Avenue Edouard Belin, Toulouse 31400, France

2. Environmental Protection, Saudi Arabian Oil Company, Dahahran, Saudi Arabia

3. Ali I. Al-Naimi Petroleum Engineering Research Center, KAUST, Saudi Arabia

4. OPC consulting, London, United Kingdom

5 Institute of Earth Sciences, University of Iceland, Sturlugötur 7, 102 Reykjavík, Iceland

* Corresponding author: eric.oelkers@cnrs.fr

Abstract

The Jizan region of southwest Saudi Arabia contains large industrial point sources of CO_2 and potentially the capacity to dispose substantial quantities of this gas by the subsurface mineralization of local basaltic rocks. Monte Carlo estimates suggest that the total CO_2 mineralization capacity of the mafic igneous rocks in the Jizan area is ~4.2 Gt CO_2, which is sufficient to store all of the carbon emissions from the local industrial facilities for four hundred years. Significant volumes of basalt were erupted in the region during the late Oligocene in a continental rift before the opening of the Red Sea. These rocks consist of lava flows and volcaniclastics intruded by dikes and shallow plutons. They are densely fractured and variably altered to chlorite-epidote-calcite assemblages.

Dissolution rate measurements performed at 25 °C of four variably altered basaltic rocks from the region demonstrate their ability to increase fluid pH and liberate substantial Ca and Mg to the fluid phase. Reaction path calculations suggest that water charged CO_2 will readily carbonate when interacting with the basaltic rocks at both 25 and 100 °C. Reactive transport calculations, however, suggest that while such carbonation reactions will be slow at 25 °C, these would fix more than 95% of injected water-dissolved CO_2 within five years at 100 °C. Taken together, the

results of this study indicate the likely success of large-scale subsurface carbon storage efforts through the subsurface carbonation of basaltic rocks in the Jizan region.

1. Introduction

This study is motivated by the current societal priority to limit carbon dioxide emissions to the atmosphere (e.g., Broecker, 2007; Yann et al., 2018; IPCC, 2021). Recent models suggest that as much as 10 Gt/year of CO_2 must be captured and stored to maintain global climate within 1.5 ^oC of its preindustrial levels (Rogelj et al., 2018). The storage of this much carbon will require large disposal volumes. For example, the volume required to store one Gt of CO_2 as either a pure supercritical phase or within a mineral such as calcite is roughly 1 km^3. The need for such large storage volumes has motivated efforts to identify suitable subsurface geologic disposal options. Major industrial CO_2 emission sources are located in various parts of the world. In some areas these sources are located in sedimentary basins containing sealed saline aquifers that are suitable for CO_2 disposal (e.g., Kongsjorden et al., 1998; Michael et al., 2010; Wurdemann et al., 2010). In other areas, targeting reactive rocks to induce subsurface mineral carbonation may provide a safe and cost-effective alternative carbon disposal solution (Gislason and Oelkers, 2014; Matter et al., 2016; Snæbjörnsdóttir et al., 2020).

The goal of this study is to generate a disposal option for the carbon emissions originating from the major CO_2 sources located in the southwestern region of Saudi Arabia. Those sources include the petroleum refining, power generation and desalination facilities of the Jizan Economic City (JEC) and the Shuqaiq desalination and power generation plant (Figure 1). It is estimated that the JEC will generate as much as 38 million tons of CO_2 emissions annually. A challenge to addressing these emissions is that the Jizan Economic City is located far from the vast sedimentary basin in Eastern Saudi Arabia. The region however is rich in rocks of basaltic compositions, which could potentially promote the subsurface mineralization of CO_2 emissions captured from the Jizan Economic City.

Carbon storage by subsurface mineralization in reactive mafic rocks is a relatively new technology. This process was first demonstrated in Iceland as part of the CarbFix project, where ~200 tons of CO_2 was dissolved into water during its injection into fresh subsurface basalts. Regular monitoring

and geochemical calculations showed that more than 95% of the CO_2 injected into these rocks having a subsurface temperature of ~35 ^oC was mineralized within two years (Matter et al., 2016; Snæbjörnsdóttir et al., 2017, 2018a). This effort has subsequently been upscaled to capture and store more than half of the CO_2 and all of the H_2S emitted from the Hellishedi powerplant since 2014 as part of the CarbFix2 project (Gunnarsson et al., 2018; Clark et al., 2020). In this latter effort both CO_2 and H_2S were captured directly from the power plant emissions by their dissolution in water within a scrubbing tower. The CO_2 and H_2S charged water was injected without depressurizaion into a subsurface aquifer containing altered basalts located at a depth of 800 m and having a temperature of ~250 ^oC. More than 50% of the CO_2 and all of the H_2S injected into this system was observed to have been mineralized within 4 months of its injection. An alternative subsurface mineralizaion approach was adopted at the Wallula basalt demonstrataion project in the United States, where 1,000 tons of pure liquid CO_2 was injected into Columbia river basalts (McGrail et al., 2014). Geophysical monitoring and modelling indicated that a substaintial part of the injected CO_2 was mineralized within two years (McGrail et al., 2017). Each approach to subsurface mineralization offers its advantages and disadvantages. In the CarbFix approach, the dissolution of the CO_2 into water prior to or during its injection 1) removes the buoyancy of the carbon such that the presence of impermeable cap rocks is not necessary, and 2) accelerates the subsurface carbonation reactions. In contrast, the Wallula approach requires only the injection of supercritical CO_2 potentially limiting injection costs.

This study is a part of a broader initiative to evaluate the CO_2 sequestration potential of basaltic volcanic and subvolcanic rocks the Jizan region. Towards this goal, the geology and structure of the subsurface has been reviewed, representative rock samples have been collected and analyzed, the reactivity of selected samples has been measured in the laboratory and geochemical modeling has been performed to assess the likely fate of water-dissolved CO_2 injected into the Jizan subsurface. The purpose of the present communication is to report the results of this field, experimental, and computational study illuminating the possibility of subsurface mineral storage of CO_2 in the Jizan region of Saudi Arabia. Detailed studies on the structural geology, petrology, and geochemistry of the Jizan rocks will be presented separately.

2. Geologic setting

The geology of the Jizan coastal region is dominated by continental rifting that preceded the opening of the Red Sea (Schmidt et al., 1983, Hughes and Johnson, 2005; Tapponnier et al., 2014). Of interest for mineral carbonation are the Oligocene basalts of the Jizan Group and the sheeted basalt dikes of the Tihamat Asir complex which intrude them. These rocks filled the southern part of the Oligocene continental rift and extend along the coastal plain from Yemen to Jeddah (Pallister, 1987, Torres, 2020). In the Jizan region these rocks are exposed in Wadis along the eastern side of the coastal plain about 20 to 30 km inland from the Red Sea (Fig. 1a). The surface geology of the area was mapped and described by Blank et al. (1986), Bohannon (1987) and Voggenreiter et al. (1989). This was combined with published and unpublished seismic and well data (e.g., Ahmed, 1972) and our field studies to produce the geologic map and cross section in Figure 1 (Torres, 2020).

The stratigraphy of the Jizan Group was described by Schmidt et al. (1983) and Schmidt and Hadley (1983) as a sequence of bimodal volcanic and volcanoclastic rocks that filled the continental rift during the Oligocene. It consists mainly of basalt lava flows, agglomerates, and tuff-breccias of the Ad Darb and Damad Formations. These are interspersed with dacitic-rhyolitic lavas and ignimbrites of the Liyyah Formation and the lacustrine siliceous tuffs of the Baid Formation, which contains fossils of fresh water fish (Tilapia sp.) and vertebrates. The Jizan Group uncomfortably covers the Precambrian basement and erosional remnants of Paleozoic and Mesozoic sedimentary rocks. It is overlain with angular unconformity by Miocene and younger post-rift clastic sedimentary rocks and evaporites. The thickness of the Jizan Group is variable and poorly resolved on seismic data. It fills seaward-tilted half grabens (Figure 1b) and its exposed thickness ranges up 2,000 m (Schmidt et al., 1983).

The volcanics of the Jizan Group and older rocks are intruded by dense swarms of basalt dikes which trend N to NW and dip between 60 to 90 degrees east. These intrusive rocks are called the Tihamat Asir dike swarm (Coleman et al., 1983) and are dated 21-24 Mya by Sebai et al. (1991). The dikes are mainly basalt, diabase, and gabbro. In some areas, the basalt dikes are closely spaced with few or no rock screens between them, similar to sheeted dikes in ophiolites (Coleman et al., 1983). Based on paleomagnetic measurements, Kellogg and Blank (1982)

determined that the basalt dikes have been rotated by ~20 degrees towards the Red Sea. In addition to the dikes, there are small plutons of layered gabbro and granite that intrude the basement and Jizan Group, the most notable at Jabal at Tirf east of Jizan (Figure 1). Torres (2020) observed that these plutonic rocks were clustered along the base of the Jizan Group (figure 1), and that they are compositionally similar to the Jizan Group, and considered them as shallow magma chambers that fed the volcanics.

The basalts of the Jizan group contain primary phenocrysts of plagioclase, clinopyroxene, and magnetite, but lack olivine. They are variably altered to secondary albite, chlorite, calcite, epidote, hematite, and pumpellyite which are indicative of hydrothermal metamorphism. However, most of the intrusive dikes and gabbros are relatively unaltered, and it is likely that their intrusion caused the hydrothermal alteration of the volcanics (Torres, 2020). Outcrop studies by Al Malalah (2021) and Fedorik et al. (in preparation) reveal that the Jizan Group is highly faulted and densely fractured in several directions. These fractures are essential to provide permeability for injection of CO_2 charged waters in the subsurface, particularly because primary porosity in vesicles, breccias, and interflow layers was largely plugged by hydrothermal minerals. There are several active and inactive hot springs in the area (Berthier et al., 1981), which also indicate the presence of deep open faults and fractures in the subsurface.

3. Methods

3.1 Field sampling and rock analysis

Thirty rock samples were collected during field work in the area in 2019. A total of 14 samples of volcanic and subvolcanic (dike) rocks were selected for detailed analysis. The mineralogical and geochemical compositions of these samples were determined by optical and reflected light microscopy, semi-quantitative X-Ray Diffractometry (XRF), and by a whole rock X-Ray Fluorescence (XRF) analyses. The analytical methods are described below.

X-Ray powder diffraction: Samples were dried at 60ºC and grinded to grain sizes smaller than 0.062 mm. The analyses were done on a BRUKER D2 PHASER powder diffractometer at 30 kV, intensity of 10 mA and Kα1 λ° = 1.54060 Å Cu radiation. The data was processed using

DIFFRAC.EVA software. The proportions of individual minerals obtained from highly alerted and/or weathered samples using this method can be impacted by refinement errors (e.g. preferential orientation of certain minerals in the samples) as well as by the presence of poorly crystalline or non-crystalline (amorphous) phases in the rocks. Therefore, results for such samples should be regarded as semi-quantitative, maximum values. In an attempt to improve resolution, highly altered/weathered samples were crushed and reanalyzed by using Rietveld refinement. The structures of the crystalline phases in those samples were processed by minimizing the difference, calculated by the least squares method, between a calculated theoretical diffraction pattern and the measured one. A known percentage (10 to 20 wt.%) of a zincite (ZnO_2) reference phase was added to each sample for quantification and to check the reliability of results. The powdered mixture was homogenized prior to mounting onto randomly oriented powder sample holders. Measurements were performed on the same equipment and the measurements were performed at θ/2θ between 2 and 70° with steps of 0.02° with a measuring time of 1 s per step. Results were processed using the FullProof Suite software. The mineral structural entry data for the theoretical model have been obtained from the Crystallography Open Database. The peak profile used is a Pseudo-Void function.

X-Ray Fluorescence (XRF): The samples were finely grounded and introduced to XRF sampling cups, sealed with 4 micron thick polypropylene film. Elemental analyses were performed on a wavelength dispersive X-ray fluorescence spectrometer, model S4 Pioneer of Bruker AXS GmbH under helium atmosphere. A 4 kW excitation technology and optimized beam geometry was used to improve sensitivity for the light and trace elements. Analytical performance for light elements was optimized by using a thin Beryllium tube window in combination with optimized excitation parameters. Estimated uncertainties are on the order of ±1% of the reported value. The Loss on Ignition (LOI) was determined by using a Carbolite muffle furnace and an electronic analytical balance Mettler-Toledo XP-205.

3.2 Experiments to assess rock reactivity of the Jizan basaltic rocks

Selected rock samples were cut and crushed. Each sample was dry sieved to obtain the 50 to 100 µm size fraction. This fraction was then repeatedly cleaned ultrasonically in ethanol.

Between each ultrasonic cleaning the particles were allowed to settle for 20 minutes. The resulting crushed rock powders were then dried overnight and kept at ambient temperature before being used in the experiments.

Batch experiments were performed in 250 ml polypropylene Nalgene reactors. Into each reactor was placed 2 gm of crushed cleaned rock sample and 248 g of a pH 3 aqueous HCl solution. This fluid pH was selected so that it would have a similar pH to likely CO_2 charged injection waters. The reactors were sealed and placed into a 25 ± 1 ^{o}C shaking water bath. At selected times, 2 g samples of the reactive fluids were collected from each reactor using a 0.22 μm filtered syringe. Fluid samples were immediately acidified to 2% HNO_3 for subsequent elemental analysis using a Varian 720-ES ICP-OES. The estimated uncertainties on these analyses are ±2%. The reactive fluid pH was measured using a Mettler Toledo LF422 pH probe with an accuracy of ±0.02 pH units at the time of each sampling.

3.3 Reaction path and reactive transport modelling

The potential for mineral carbonation is assessed in this study though the use of reaction path and reactive transport calculations. All calculations were performed using the PHREEQC software package (Parkhurst and Appelo, 2013) together with the *carbfix.dat* (v1.1.0) thermodynamic database (Voigt et al., 2018). The compositions, chemical formulas, molar volumes and thermal stability fields of the secondary phases considered in the calculations are listed in Table 1. This list was adopted from Marieni et al. (2021b) and it is based on the minerals observed in naturally altered basaltic rocks and those observed in fluid-basalt interaction experiments. The thermal stability fields in Table 1 defines the temperature range in which a mineral has been observed in experimental and/or field studies. Consistent with field observations, dolomite was not allowed to precipitate, and the formation of aqueous reduced carbon species and methane (CH_4) was restricted.

3.3.1 Reaction path calculations

To assess the fate of water dissolved CO_2 into the basaltic rocks, reaction path calculations were performed where a 0.1 molal NaCl aqueous solution was initially charged with 10 bar of

CO_2 pressure. A fixed quantity of the rock is added to one kg of this CO_2-charged water sequentially. The model calculates the fluid speciation and the saturation state of each potentially forming mineral as the basalt is titrated into the system. For the calculations in this study the minerals listed in Table 1 were allowed to precipitate from the aqueous solution at local equilibrium if they become supersaturated. Such calculations provide a first estimate of the order and identity of minerals that might form during basalt-CO_2 charged water interaction.

3.3.2 Reactive transport calculations

The current state of the art in calculating the temporal evolution of a mineral-water system is limited by our understanding of the reaction rates. Whereas there is a large and detailed set of mineral dissolution rates measured in the literature (c.f. Palandri, and Kharaka, 2004; Marini 2007), there are nearly no measured precipitation rates of the major secondary minerals. As such the calculations generated in this study are based on the assumption that all minerals allowed to precipitate do so at local equilibrium. This assumption will lead to significant uncertainties in the calculated results, as the precipitation rate behaviors observed in the laboratory vary greatly from mineral to mineral. Whereas some minerals like calcite are observed to precipitate readily in laboratory experiments and in natural systems, other minerals like dolomite and magnesite, are not observed to precipitate at temperatures less than ~80 ^{o}C (e.g., Saldi et al., 2009). So too quartz does not precipitate at ambient temperatures. Moreover, the precipitation rates of many Al-bearing clay minerals are sluggish (e.g. Nagy et al., 1991; Yang and Steefel, 2008; Schott et al., 2009), though not well quantified. Such uncertainties limit greatly the precision of any temporal mineral-fluid calculation.

Although the literature of experimentally measured dissolution rates is extensive, these experimental rates exhibit much scatter and they must be considered to have uncertainties ranging toward 1 order of magnitude (cf. Brantley, 2003; Palandri and Kharaka, 2004; Marini, 2007; Sverdrup et al., 2021). These rates have been shown to depend on the fluid composition fluid pH, the chemical affinity of the dissolving mineral and the mineral-fluid interfacial surface area. Rates used in the calculation of this report come from the internally consistent kinetic database for the PHREEQC code generated by Hermanska et al. (2022).

The calculation of the temporal evolution of a mineral-fluid system is complicated by the need to define the surface area of the dissolving minerals. These surface areas will depend greatly on the hydrology of the system (cf. Oelkers, 1996). For example, the surface area of a fluid flowing through a 1 mm wide smooth fracture will have a mineral surface area of 2 m^2/kg(H_2O). If this fracture is not smooth one might expect this surface area to increase to something on the order of 8 to 10 m^2/kg H_2O. In contrast, if the flow is through a porous rock consisting of 1 mm grains with a 10% porosity one might expect a surface area on the order of 100 m^2/kg H_2O.

To allow for a representative estimate of the reactivity of the Jizan basaltic rocks, we will focus on the evolution of the fluids and mineral precipitated in a 1 mm wide crack, though which the fluid is travelling 20 m/yr. The relative surface areas of the minerals in the rock will be set to their relative volume fraction and the total surface area is set to 8 m^2/kg H_2O. The Lagrangian approximation was adopted to account for the spatial distribution of precipitated phases in the system (Lichtner 1985; 1996). Only pure advective transport is considered; the contribution of diffusion, dispersion, and subsurface fluid mixing are not taken into account, although each could have a contribution to the natural subsurface system. As the water is moving through the fracture, secondary minerals that form will not dissolve in response to the fluid compositional changes observed downstream from where these secondary minerals precipitated.

4. Results

4.1 Jizan basaltic rock compositions

The mineral and whole rock chemical compositions of the 14 basaltic rock samples analyzed are listed Tables 2 and 3. The compositions and mineral proportions determined from XRD are for the most part consistent with the optical examinations and whole rock analyses of the samples. The elevated proportions of quartz in some volcanic samples reported in Table 2 is explained by the presence of significant quantities of amorphous material (e.g. Fe and Al-rich phases). Amorphous phases are commonly reported from weathered basalts elsewhere (c.f. Smith, 2016; Lewis et al., 2021). Since these are difficult to identify, their presence will increase artificially the proportions of the identifiable crystalline phases in the X-Ray diffractograms, which appears to be the case with some of Jizan volcanic rocks reported in Table 2. Attempts to improve

resolution by using Rietveld refinement had only limited success. Therefore, the mineral proportions reported in Table 2 should be regarded as maximum values.

In thin sections, the Jizan Group volcanic rocks are generally fine-grained massive to porphyritic or vesicular with millimeter-sized phenocrysts groundmass, whereas the Tihamat Asir dikes exhibit medium to coarse-grained, predominantly phaneritic (holocrystalline) gabbro/dolerite textures. The alteration of the volcanic rocks resulted in the nearly complete loss of their volcanic glass and much of their primary minerals. As a result, the principal mineral in the volcanic rocks is Na-plagioclase (albite) and with lesser augite, quartz, epidote, titanite, Fe-chlorite (chamosite) and potassium feldspar. These samples also contain minor amphibole (actinolite), as well as prehnite, zeolite, hematite and calcite (Table 2). Those mineral assemblages indicate that the volcanic rocks have been altered at temperatures of about 300^{o}C, likely during the emplacement of the Tihamat Asir dikes and other intrusive rocks.

As reported in the literature, the dikes are less altered than the volcanics. The mildly altered to unaltered dikes consist almost entirely of Ca-plagioclase (labradorite) and clinopyroxene (augite) with subordinate Fe- and Ti- oxide minerals (i.e. magnetite, Ti-magnetite). The more heavily altered dikes contain albite, amphibole (actinolite, hornblende), chlorite and epidote. Some dike samples also contain prehnite, zeolites (analcime, epistillbite) and calcite (Table 2).

The low SiO_2 content of the samples is consistent with their basaltic origin (Table 3). On the basis of their alkaline element contents, the rocks vary in compositions from alkaline basalts (basanite) to basaltic trachyandesites, with the Jizan Group volcanics exhibiting greater variability, while most dike samples fall into the basanite group (Table 3; Fig. 2). The CaO, MgO, and Fe_2O_3 contents of these rocks, which range from 3.5 to 11.2, 1.6 to 8.1 and 10.2 to 15.1 wt. %, respectively, indicate that these could be good sources of the divalent cations needed for the mineral carbonation of injected CO_2.

Four rock samples (JG 202, WJU 01, WJS 02 and WJU 03) were selected for laboratory reactivity studies. The first two are volcanic rocks collected from the Jizan Group, while the other two are Tihamat Asir dikes. Because of their different origins and variable degree of alteration and hence mineral contents, the samples are considered representative of the predominant basaltic lithologies in the Jizan region (Table 2).

4.2 Experimentally measured Jizan rock reactivities

Temporal evolutions of the pH and reactive fluid Si concentrations of all experiments performed in this study are presented in Fig 3. Each batch experiment lasted from 60 to 80 days. The interaction of the samples with mildly acidic solutions leads to the relatively rapid increase in fluid pH and a continuous increase in the aqueous fluid Si concentration. In each experiments the fluid pH increased rapidly from ~3 to more than 6.

The Si release rates from each experiment were fit assuming that their rates could be described as a linear function of pH in accord with

$r = ksa_{H^+}^{n}$ (1)

where *k* refers to a rate constant, *s* designates the geometrically calculated surface area of crushed rock in the reactor, *n* stands for a reaction order, and a_{H^+} denotes the activity of H^+ in the reactive aqueous fluid. The surface area used in these calculations are the geometric surface areas of the rock samples, which was taken to be 0.23 m^2/g, assuming the grains to be spherically shaped and the average of the 50 to 100 µm diameter basalt grains used in the experiments. Measured aqueous Si concentration during the experiments were fit to Eqn. (1) by first fitting measured fluid pH as a function of time to a logarithmic fit equation. The quality of the resulting temporal pH fits equations can be assessed in Fig 3. The temporal pH fit equation was then used to numerically integrate Eqn (1) to generate the values of Si concentrations shown by the curves in Fig. 3. The obtained values of *k* and *n*, which are provided in Table 4, were generated by trial and error to obtain the best fit of measured reactive fluid Si concentrations in each experiment. A close correspondence can be seen between the measured and calculated Si concentrations.

Table 4 reports Si release rates as determined from Eqn. (1) and the parameters provided in this table. The measured Si release rates are similar for all of the samples, and range from $10^{-9.3}$ to $10^{-8.8}$ $mol/m^2/s$ at pH 4 and $10^{-10.1}$ to $10^{-11.1}$ $mol/m^2/s$ at pH 6. Overall, a good reproducibility is observed between duplicate experiments performed on the same powders.

A summary of the relative release rates of Ca and Mg relative to that of Si are presented in Fig. 4. It can be seen that there is a rapid initial release of calcium and magnesium to the fluid phase in all experiments. Although the relative concentration of these elements tends to

decrease with time, the [Ca]/[Si] molar ratios generally remain more than an order of magnitude higher than that of the dissolving rock throughout the experiments, whereas the corresponding [Mg]/[Si] molar ratios tend to remain on average a half an order of magnitude higher than that of the dissolving rocks. The preferential release rates of these elements persist throughout the experiments. In contrast, the measured dissolved Fe and Al concentrations were at or below the detection limit in all measured samples, likely reflecting the rapid precipitation of these phases in sparingly soluble metal hydroxide phases.

4.3 Geochemical modelling

4.3.1 Reaction path modelling

Taking account of the compositions of the rock samples collected and analyzed in this study (Table 2), a rock containing 65% albite, 15% clinopyroxene 10% epidote and 10% chlorite was reacted, with the aid of the PHREEQC software, with a 0.1 M NaCl solution charged with 10 bars of CO_2-charged water as a function of the mass of rock dissolved. This rock is similar in composition and mineralogy of the moderately altered rocks described in Tables 2 and 3. Each mineral in the rock is assumed to dissolve stoichiometrically into the fluid phase at a relative rate proportional to its volume fraction. All potential secondary minerals are allowed to precipitate at local equilibrium. Minerals that might become supersaturated but not observed to form in nature, such as pure end-member pyroxenes, however, were not allowed to form in the calculations, consistent with the list of minerals listed in Table 1. Results of this reaction path calculation for a fluid-rock system at 25 and at 100 ^{o}C are shown in Figs. 5 and 6.

At 25 ^{o}C the pH of the initial CO_2 charged saline water was 3.4 and contained 0.32 mol/kg of CO_2. The interaction of this water with the dissolving altered Jizan basalt provokes an increase in pH to ~10 as 1 mole of this rock dissolves. The reaction between the fluid and rock leads to the supersaturation and precipitation of a number of secondary minerals. A suite of smectite clay minerals, nontronite and beidellite, begin to precipitate once 10^{-4} moles of altered Jizan basalt rock/kg H_2O has dissolved. Calcite begins to precipitate after ~0.01 mol/kg H_2O of the altered basalt has dissolved, and some zeolites, notably mordenite, thomsonite and analcime are computed to precipitate after 0.001 mol/kg H_2O of sample dissolved. As the result of the calcite

precipitation, all of the injected carbon is eventually captured and stored as in this mineral. This can be visualized in the center diagram of Fig. 5, where is can be seen that essentially all of the dissolved carbon has been removed from the aqueous phase before 1 mol/kg H_2O of rock has dissolved.

A corresponding calculation for the dissolution of altered basalt at 100 °C is shown in Fig. 6. These results are similar to those generated for the 25 °C fluids with several distinct differences. First, the total amount of CO_2 dissolved into the initial water was ~3 times lower than that at 25 ^oC reflecting the retrograde solubility of this gas in water. Diaspore is calculated to form after $1x10^{-4}$ mol/kg H_2O of altered Jizan basalt dissolves. Its presence at 100 ^oC compared to 25 ^oC is due to the lower initial CO_2 concentration of the injected fluid and thus lower acidity of the initial system; the pH of the initial fluid is 3.65, slightly less acidic than the initial fluid at 25 ^oC. Note that diaspore is calculated to be the most stable Al hydroxide phase at this temperature and pressure condition. Its stability is similar to that of boehmite and gibbsite, so in natural systems one or the other might form in the place of diaspore. The exact identity of the Al-hydroxide phase formed in the model calculation changes negligibly the computed evolution of the water-rock system. As observed at 25 ^oC, beidellite clay begins to precipitate after $1x10^{-4}$ mol/kg H_2O of rock dissolves followed by other clay minerals. Calcite begins to precipitate after 0.01 mol/kg H_2O of rock dissolved. The total amount of calcite formed at 100 ^oC is approximately 3 times less than that formed at 25^o C due to the lower initial mass of CO_2 in the fluid. Zeolites begin to appear after 0.1 mol/kg H_2O of rock dissolves. Additional reaction path models were run to assess if the use of seawater rather than a dilute saline water would alter substantially the secondary mineral formation and carbon consumption in this system. The use of seawater for CO_2 dissolution and injection changes little the carbonation potential of the hypothetical rock at both 25 and 100^o C compared to that in the dilute aqueous NaCl solution considered in the above calculation.

4.3.2 Reactive transport modelling

Insight into the potential time required for the carbonation of CO_2-charged water injected into the mafic volcanic and subvolcanic rocks can be gained though reactive transport

calculations. Results from the reaction of a 0.1 m/kg NaCl aqueous solution charged with 10 bars of CO_2 pressure injected into a fracture within altered Jizan basalts at 25 ^oC are shown in Fig. 7. The results shown in this figure span over 100 years with the injected CO_2 charged water flowing at a rate of 20 m/year within a 1mm wide fracture. During this time, injected water moved 2 km through the fracture. The dissolution of the altered Jizan basalt is dominated by the dissolution of albite. Despite the presence of substantial augite, epidote and chlorite in this rock, these minerals contribute relatively little mass to the fluid phase as their dissolution rates are substantially lower than those of albite. The dissolution of altered Jizan basalt increases the pH of the injection fluid from ~3.4 to ~6.0 over the course of 100 years. The rate at which albite dissolves decreases with time and distance in the fracture as the dissolution rates slow due to increasing fluid pH. Similar to the corresponding reaction path model (see Fig. 5), the mass of secondary minerals formed are dominated by the formation of clay and zeolite minerals, identified here by the clays beidellite and montmorillonite, and the zeolite mordenite. Amorphous SiO_2 is calculated to be the dominant SiO_2 phase; although quartz and calcedony are more stable thermodynamically, these were not allowed to precipitate in the model calculation to be consistent with field observations (Neuhoff et al., 2010). Only minor carbonate minerals are calculated to form. Calcite remained undersaturated during the simulation, minor siderite was calculated to precipitate. The amount of siderite calculated negligibly changed the total dissolved carbon in the injected fluid during the 100-year simulation. Despite the low degree of carbonation, the partial pressure of CO_2 of the fluid phase decreased from 10 to 6 bars over time due to the increased pH of the system.

The results of corresponding calculations for the injection of a CO_2-charged aqueous 0.1 m NaCl solution into a 1 mm fracture of altered Jizan basalt at 100 ^oC are shown in Fig. 8. The dissolution of the altered basaltic rocks at this temperature is dominated the dissolution of both albite and augite. The dissolution rate of albite decreases to near zero after ~3 years and the fluid has traveled 60 m. At this point the fluid approaches equilibrium with albite arresting its dissolution. The fluid, however, remains significantly undersatured with respect to augite until the dissolved carbon concentration decreases to below ~10^{-3} mol/kg. As the relative rates of albite versus augite changes as the fluid interacts with the Jizan rock along the flow path, the

major Ca bearing secondary phase changes from the aluminum bearing zeolite, Ca mordenite, to the carbonate calcite. Again, in this calculation the secondary minerals epidote and chamosite contribute relatively little material to the aqueous phase due to their slower dissolution rates.

In contrast to the corresponding calculation for the 25 ^{o}C system, substantial carbon dioxide mineralization is observed in the 100 ^{o}C simulation. Carbonate mineral formation is calculated to begin within the first month of the injection at 100 ^{o}C and dominated by the precipitation of siderite and magnesite for the first seven months after injection. From months 8 to 12 the carbonate ankerite is calculated to dominate carbon mineralization, whereas after this time, calcite precipitation is calculated to dominate carbon mineralization. As a result of the precipitation of these carbonate minerals, the roughly two third of the originally injected CO_2 is calculated to be mineralized within 3 year and over 95% within 5 years. Moreover, as the pH increases as the Jizan basalt dissolves, the partial pressure of CO_2 in the fluid phase drops below its partial pressure in the atmosphere after only 2.6 years.

The secondary minerals calculated to precipitate are dominated by the precipitation of the zeolite mineral Ca-mordenite during the first 8 months, whereas saponite clay is calculated to be the most voluminous secondary mineral after this time. The calculated net mineral volume change due to the combined effects of primary mineral dissolution and secondary mineral precipitation are close to zero for most of the fracture, with the exception of near the inlet. This result suggests that the fracture system should remain open for extended time during the injection of carbon dioxide charged water.

5. Discussion

5.1 The relative release rates of metals from the Jizan basaltic rocks.

A notable aspect of the experimental rate measurements is the initial fast release of Ca and Mg compared to Si to the fluid phase. There are several potential reasons for the relatively rapid release of Ca and/or Mg at the beginning of the experiments. First, these metals could be sourced from the presence of a minor rapidly dissolving phase, such as a carbonate mineral in the rock phase. Although calcite was not detected in these samples, minor secondary calcite is found in some of the rock samples (see Table 2). The early rapid release of both Ca and Mg could also be

the consequence of metal for proton for exchange reactions from the fresh mineral surfaces exposed to the initial acidic fluid phase. The preferential early release of Ca and Mg from the surfaces of pyroxene minerals was reported at acid pH by Oelkers et al. (2009) and attributed to such exchange reactions. A similar rapid release of Ca from epidote has been reported by Mareni et al. (2021). These exchange reactions may also be the source of the rapid increase in pH observed in the experiments. The continued preferential release of Mg and Ca from the Jizan rocks after the first part of the experiments may reflect the preferential dissolution of Mg and Ca rich phases in the rocks. For example, the preferential dissolution of pyroxenes would favor the preferential release of these elements. It should be noted, however, that this preferential release is not observed in the results of reactive transport model calculations performed in this study, which suggest that plagioclase would tend to be the mineral dominating the dissolution of the Jizan basalts at 25 ^{o}C.

5.2 Comparison of the results of reaction path and reactive transport calculations

Both reaction path and reactive transport calculations were run at identical conditions in this study. Nevertheless, although the results of the distinct calculations are similar in some aspects, they differ in some other aspects. In each case, the interaction of the injected CO_2 charged aqueous NaCl solution provokes the dissolution of the original altered rock, leading to an increase in the fluid pH. As the concentration of dissolution products build up in the fluid phase secondary minerals precipitate dominated at first by the formation of smectite clays and zeolite.

The calculations for the 25 ^{o}C system, however, exhibit significant differences in terms of the carbon-dioxide fixation potential for the Jizan basaltic rocks. The reaction path calculation suggest that the fixation of the injected CO_2 would begin to carbonate after ~0.1 moles of altered Jizan basalt dissolved into the fluid, and carbonation would be close complete after less than a mole of rock had dissolved. In contrast, only negligible mineral carbonation was observed in the corresponding reactive transport calculation over the 100-year duration of the simulation. The major reason for this apparent difference is the slow dissolution rates of the divalent metal bearing minerals in the altered Jizan basalt. Over the 100-year duration of the reactive transport simulation, 0.13 moles/kgw of albite was calculated to dissolve but only 0.02 moles/kgw of augite

and less than 0.005 moles/kgw of either epidote or chamosite. The relatively slow dissolution rates of these minerals in the not only limits the release rates of the divalent metals required for the formation of carbonate minerals, but also preferentially releases Al to the fluid phase compared to the composition of the bulk altered Jizan basalt. The preferential addition of Al to the fluid phase favors the formation of Al-bearing secondary minerals such as clay and zeolite minerals compared the carbonates.

Similarly, the 100 ^{o}C reaction path model calculation also yields somewhat different results compared to the reactive transport model calculation in terms of mineral carbonation. At this temperature the only carbonate to form in the reaction path calculations is calcite, which begins to precipitate after ~0.03 mol/kgw of altered basalt has dissolved (Fig. 6); carbonation of the injected CO_2 is complete once one mole of this basalt has dissolved into each kg of injected CO_2 charged fluid. In contrast, the reactive transport model predicts a suite of carbonate minerals will form, starting with siderite and magnesite within the first month after fluid injection. These carbonate minerals begin to precipitate after less than 0.03 moles/kgw of the altered basalt begins to dissolve. These carbonate minerals are followed by the precipitation of ankerite, and finally calcite after ~0.15 mol/kgw of the altered basalt had dissolved approximately one year after the injection of the CO_2 charged fluid (Fig 8.). At this point the fluid pH is ~8.5 and albite is close to equilibrium with the fluid phase, so augite dissolution is relatively fast. At these conditions there is relatively less Al but more divalent cations being released to the aqueous solution, favoring the formation of secondary carbonate rather than Ca-bearing zeolite minerals.

5.3 Comparison of experimentally measured element release rates with reactive transport calculation results.

The experiments performed in this study determining the element release rates from the selected samples can be compared directly to those obtained from the 25 ^{o}C reactive transport calculations. The Si release rates of the experiments at pH 6 were determined to range from and $10^{-10.1}$ to $10^{-11.1}$ mol Si/m^2/s. This compares to the calculated Si release rates of $10^{-10.86}$ mol Si/m^2/s determined in the reactive transport calculations. This coherence in rates supports both 1) the use of the Hermanska et al. (2021) mineral dissolution rate database to estimate the

carbonation of altered Jizan basalts, and 2) the estimated volume percentage of the mineral present in the altered Jizan rocks used in the geochemical calculations.

A noteworthy difference between the experimental results and the reactive transport calculations is the relative release rates of the divalent cations Ca and Mg. In the experiments, these elements were preferentially released to the fluid phase compared to Si both initially and throughout the duration of the experiments. In contrast, in the 25 ^{o}C reactive transport calculations these elements are preferentially retained by the altered basalt due to the relatively fast dissolution rate of albite compared to the other primary minerals present in the system. In the calculations, molar Ca/Si and Mg/Si ratios released to the fluid phase are less than half of these ratios in the altered basalt. The difference between the results of the experiments and the reactive transport calculations suggest that the calculations are missing provision for the non-stoichiometric preferential release of divalent metals from the minerals present in the altered basalt, perhaps by proton for metal exchange reactions on the mineral surfaces (e.g. Oelkers et al., 2009). As Ca and Mg are elements that promote carbonation in the subsurface this difference suggests that the reactive transport calculations underestimate the carbonation potential of the Jizan basaltic rocks.

5.4 Application to the carbonation potential of the basaltic rocks of the Jizan region of Saudi Arabia.

The results summarized this this study indicate that the altered volcanic and subvolcanic rocks at Jizan have the potential to rapidly store carbon-dioxide via mineralization in the subsurface at relatively moderate temperatures of ~100 ^{o}C or more. Note, however, that several studies reported that the efficiently of mineral carbonation in basalts will decline significantly at temperatures above 250 ^{o}C. (e.g. Mareni et al., 2021b). This suggests that CO_2 injection at Jizan should target subsurface zones where the temperatures of the basaltic rocks are in the 100 to 250 ^{o}C range.

An estimate of the potential carbon storage capacity of the basaltic rocks of the Jizan region can be made using Monte Carlo calculations. Such calculations were performed in the present study using the code 'CrystalBall 3'. Taking into account the geology of the Jizan region, the surface

area occupied by basaltic rocks was estimated to have the likeliest surface extent of 150 km^2 with a minimum and maximum extent of 50 and 500 km^2, respectively. The thickness of the basalts was estimated to most likely be 1 km, with a minimum and maximum thickness ranging from 0.3 to 1.5 km. The carbon storage capacity of the Jizan basalts, based on the observed carbon mineralization capacity of Icelandic basalts was taken to most likely be 55 (kg CO_2)/(m^3 of basalt) with a range of 10 to 90 kg/m^3 (Wiese et al., 2008; Snæbjörnsdóttir et al., 2014). The accessibility of the basalt to the injected CO_2-charged water was taken to range from 10 to 90% with the most likely accessibility being 40%. A triangular distribution of each potential was considered in the storage capacity. The median storage capacity of the Jizan basalts estimated through the calculation was 4.2 Gt, with a 10% probability that this capacity would be less than 1.4 Gt or more than 10.2 Gt. It is estimated that the Jizan Economic City will generates 10 million tons of CO_2 annually (Vahrenkamp et al., 2021). The storage capacity estimates made in the present study indicate that the basaltic rocks of this region will have the capacity to store from 140 to 1000 years of CO_2 emissions generated from the Jizan Economic City as stable carbonate minerals.

6. Conclusions

This study of the basaltic rocks of the Jizan region of southwest Saudi Arabia indicate that these rocks have the potential to store substantial carbon-dioxide through surface mineralization reactions. Notably:

1) Experimental rate measurements performed at 25°C show that four representative samples of variably altered basaltic rock exhibit Si release rates that match those calculated using mineral dissolution rates available in the literature. This coherence suggests that we can use these existing mineral dissolution rates with confidence to assess the temporal fate of CO_2 charged waters injected into these rocks.
2) Reaction path models suggest the altered Jizan rocks should carbonate at both 25 and 100 °C in response to the injection of both CO_2-rich fresh water and/or seawater.
3) One-dimensional reactive transport model calculations suggest that the injection of CO_2 charged seawater into a 1 mm wide fracture in altered basaltic rock will fix the injected carbon into newly formed carbonate minerals within 5 years at 100°C. At 25 °C this

process may take in excess of 100 years. Rates will, however, be accelerated in hydrologic systems where the fluid flows through porous regions of the basalts where the mineral-fluid surface area could be substantially higher than in a fracture.

4) Experimental rate measurements showed a preferential release of Ca and Mg into the fluid phase, which may indicate that these metals could be preferentially released in the natural system through metal for proton exchange reactions. As the presence of Ca and Mg promote the precipitation of carbonate minerals, the mineral carbonation rates of the reactive transport calculations, which do not take account of this exchange reaction, may underestimate significantly the carbonation rates of the altered Jizan basalts.
5) The potential storage capacity of the Jizan basalts is estimated to range from 1.4 to 10.2 Gt, sufficient to store from 140 to 100 years of the CO_2 likely to be emitted from the Jizan Economic City.

Taken together these results encourage the exploitation of the basaltic rocks at Jizan for subsurface carbon disposal.

References

Ahmed, S.S., 1972. Geology and petroleum prospects in Eastern Read Sea. Am. Assoc. Pet Geo. Bull. 56, 707-719.

Alt, J.C., 1995. Subseafloor processes in mid-ocean ridge hydrothermal systems. Seafloor Hydrothermal Systems: Physical, chemical, biological, and geological interactions, 85-114.

Al Malallah, M. Y., 2021, Fracture network analysis for carbon mineralization in the Oligocene Jizan volcanics, Saudi Arabia [M.S. Master of Science]: KAUST, 88 p.

Berthier, F., Demange, J., Iundt, F., and Ver Zier, P., 1981. Geothermal Resources of the Kingdom of Saudi Arabia. Saudi Arabian Deputy Ministry for Mineral Resources, Open-File Report BRGM-OF-01-24

Blank, H. R., Johnson, P. R., Gettings, M.E., Simmons, G. C. 1986. Explanatory notes to the Geologic Map of the Jizan Quadrangle sheet 16F, Kingdom of Saudi Arabia Ministry of Petroleum and Mineral Resources, US Geological Survey Open Access Report 85-724, 25 p.

Bohannon, R.G., 1987. Tectonic configuration of the Western Arabian Continental Margin Southern Red Sea, Kingdom of Saudi Arabia. USGS Open file report 87-512,29p.

Brantley, S.L., 2003. 5.03 - Reaction Kinetics of Primary Rock-forming Minerals under Ambient Conditions, in: Holland, H.D., Turekian, K.K. (Eds.), Treatise on Geochemistry. Pergamon, Oxford, pp. 73–117.

Broecker, W.S., 2007. CO_2 Arithmetic. Science 315, 1371.

Clark, D.E., Oelkers, E.H., Gunnarsson, I., Sigfússon, B., Snæbjörnsdóttir, S.Ó., Aradóttir, E.S., Gíslason, S.R., 2020. CarbFix2: CO_2 and H_2S mineralization during 3.5 years of continuous injection into basaltic rocks at more than 250 °C. Geochimica et Cosmochimica Acta 279, 45-66.

Coleman, R.G., Brown, G.F., Keith, T.E.C. 1972. Layered grabbros in southwest Saudi Arabia. U.S. Geological Survey Professional Paper 800-D p. D143-D150.

Fedorik, J., Delaunay, A. Losi, Menegoni, Panara, Afifi, A, Al Malallah, M., Arkadakskiy, S., Ahmed, Z., Kunnummal (in preparation). Fracture characterization of Jizan Volcanics, Saudi Arabia, Journal of Structural Geology

Gislason, S.R. and Oelkers, E.H. (2014) Carbon Storage in Basalt. Science 344, 373-374.

Gunnarsson, I., Aradóttir, E.S., Oelkers, E.H., Clark, D.E., Arnarson, M.Þ., Sigfússon, B., Snæbjörnsdóttir, S.Ó., Matter, J.M., Stute, M., Júlíusson, B.M., Gíslason, S.R., 2018. The rapid and cost-effective capture and subsurface mineral storage of carbon and sulfur at the CarbFix2 site. International Journal of Greenhouse Gas Control 79, 117-126.

Gysi, A.P., Stefánsson, A., 2012. Mineralogical aspects of CO_2 sequestration during hydrothermal basalt alteration — An experimental study at 75 to 250°C and elevated pCO_2. Chemical Geology 306-307, 146-159.

Hermanska, M., Voig, M., J., Marieni, C., Declercq, J., Oelkers, E.H., 2022. A comprehensive and consistent mineral dissolution rate database: Part 1 Primary silicate minerals and glasses. Chem, Geol. (in revision).

Hughes, G. W. G., Johnson, R. S., 2005. Lithostratigraphy of the Red Sea region. GeoArabia 10, 49–126

IPCC, 2021: Climate Change 2021: The Physical Science Basis. Contribution of Working Group I to the Sixth Assessment Report of the Intergovernmental Panel on Climate Change [Masson-Delmotte, V., P. Zhai, A. Pirani, S. L. Connors, C. Péan, S. Berger, N. Caud, Y. Chen, L. Goldfarb, M. I. Gomis, M. Huang, K. Leitzell, E. Lonnoy, J. B. R. Matthews, T. K. Maycock, T. Waterfield, O. Yelekçi, R. Yu and B. Zhou (eds.)]. Cambridge University Press.

Kellogg, K.S., Blank, H. R. 1982. Paleomagnetic evidence bearing on Tertiary tectonics of the Tihamat Asir coastal plain, Southwestern Saudi Arabis. U.S. Geological Survey Open-File Report 82-1047, 40 p.

Kristmannsdóttir, H., 1979. Alteration of basaltic rocks by hydrothermal activity at 100-300 °C. Developments in sedimentology 27, 359-367.

Krìstmannsdóttir, H., Tomasson, J., 1978. Zeolite zones in geothermal areas in Iceland, in: Sand, L.B., Mumpton, F.M. (Eds.), Natural Zeolite Occurrence, Properties and Use. Pergamon Press, Oxford, pp. 277-284.

Kongsjorden, H., Karlstad, O., Torp, T. A. 1998. Saline aquifer storage of carbon dioxide in the Sleipner project. Waste Management, 17, 303-308.

Larsson, D., Grönvold, K., Oskarsson, N., Gunnlaugsson, E., 2002. Hydrothermal alteration of plagioclase and growth of secondary feldspar in the Hengill Volcanic Centre, SW Iceland. Journal of Volcanology and Geothermal Research 114, 275-290.

Lewis, A.L., Sarkar, B., Wade, P., Kemp, S.J., Hodson, M.E., Taylor,L.L., Yeong, K.L., Davies, K., Nelson, P.N., Bird, M.I., Kantola, I.B., Masters, M.D., DeLucia, E., Leake, J.R., Banwart, S.A., Beerling, D.J. 2021. Effects of mineralogy, chemistry and physical properties of basalts on carbon capture potential and plant-nutrient element release via enhanced weathering. Applied Geochem. 132, 105023

Lichtner, P.C. 1985. Continuum, model for simultaneous chemical reactions and mass trasnport in hydrothermal systems. Geochim Cosmochim Acta, 49, 799-800.

Lichtner, P.C. 1996. Coninuum formulation of multicomponent-multiphase reactive transport. Rev. Min., 34, 1-82.

Marieni, C., Voigt, M. J., Oelkers, E.H. 2021a. Experimental study of epidote dissolution rates from pH 2 to 11 and temperatures from 25 to 200 ^{o}C. Geochim. Cosmochim. Acta 294, 70-88.

Marieni, C., Voigt, M. J., Clark, D.E., Gislason, S. R. Oelkers, E.H. 2021b. Mineralization potential of water-dissolved CO_2 and H_2S injected into basalts as a function of temperature: Freshwater versus seawater. Int. J.Greenhouse Gas Cont. 109, 103357.

Marini, L., 2007. Geological Sequestration of Carbon Dioxide: Thermodynamics, Kinetics, and Reaction Path Modeling, Developments in Geochemistry. Elsevier Science.

Matter, J.M., Stute, M., Snæbjörnsdottir, S.Ó., Oelkers, E.H., Gislason, S.R., Aradottir, E.S., Sigfusson, B., Gunnarsson, I., Sigurdardottir, H., Gunnlaugsson, E., Axelsson, G., Alfredsson, H.A., Wolff-Boenisch, D., Mesfin, K., De la Reguera Taya, D.F., Hall, J., Dideriksen, K., Broecker, W.S., 2016. Rapid carbon mineralization for permanent disposal of anthropogenic carbon dioxide emissions. Science 352, 1312-1314.

McGrail, B.P., Spane, F.A., Amonette, J.E., Thompson, C.R., Brown, C.F. 2014. Injection and monitoring at the Wallula Basalt Pilot Project. Energy Proced. 63, 2939 – 2948.

McGrail, B.P., Schaef, H.T., Spane, F.A., Cliff, J.B., Qafoku, O., Horner, J.A., Thompson, C.J., Owen, A.T., Sullivan, E.C., 2017. Field Validation of Supercritical CO_2 Reactivity with Basalts. Environ. Sci. Technol. Lett. 4, 6-10.

Michael, K., Golab, A., Shulakova, V., Enis-King, J., Allinson, G., Sharma, S., Siken, T., 2010. Geologic storage of CO_2 in saline aquifers – A review of the experience from existing storage operations. Int. J. Greenhouse Gas Cont. 45, 659-667.

Nagy, K.L., Blum, A.E., Lasaga, A.C., 1991. Dissolution and Precipitation kinetics of kaolinite at 80°C and pH 3: the dependence on solution saturation state. Am. J. Sci. 291, 649–686.

Neuhoff, P.S., Fridriksson, T., Bird, D.K. 2010. Seoplite paragenesis in the North Atlantic igneous provence: Implications for geotechtonics and groundwater quality of basaltic crusts. Int. Geol. Review, 42, 15-44.

Oelkers, E.H., 1996. Summary and review of the physical and chemical properties of rocks and fluids. Reviews in Mineralogy, 34, 131-191.

Oelkers, E. H., Golubev, S. Chairat, C. Pokrovsky, O.S., Schott J., 2009. The surface chemistry of multi-oxide silicates Geochimica et Cosmochimca Acta 73, 4617-4634.

Pallister, J.S. 1987. Magmatic history of Red Sea Rifting: Perspective from the central Saudi Arabian coastal plain. Geological Soc, Am. Bull. 98, 400-417.

Parkhurst, D.L., Appelo, C.A.J., 2013. Description of input and examples for PHREEQC version 3: a computer program for speciation, batch-reaction, one-dimensional transport, and inverse geochemical calculations. US Geological Survey.

Palandri, J., Kharaka, Y., 2004. A Compilation of Rate Parameters of Water-Mineral Interaction Kinetics for Application to Geochemical Modeling 1068, 71.

Rogelj, J., Shindell, D., Jiang, K., Fifita, S., Forster, P., Ginzburg, V., Handa, C., Kheshgi, H., Kobayashi, S., Kriegler, E., Mundaca, L., Séférian, R., Vilariño, M.V., 2018. Mitigation Pathways Compatible with 1.5°C in the Context of Sustainable Development, in: Masson-Delmotte, V., P. Zhai, H.-O. Pörtner, D. Roberts, J. Skea, P.R. Shukla, A. Pirani, W. Moufouma-Okia, C. Péan, R. Pidcock, S. Connors, J.B.R. Matthews, Y. Chen, X. Zhou, M.I. Gomis, E. Lonnoy, T. Maycock, M. Tignor, and T. Waterfield (Ed.), In: *Global Warming of 1.5°C. An IPCC Special Report on the impacts of global warming of 1.5°C above pre-industrial levels and related global greenhouse gas emission pathways, in the context of*

strengthening the global response to the threat of climate change, sustainable development, and efforts to eradicate poverty, *In Press*.

Rose, N.M., 1991. Dissolution rates of prehnite, epidote, and albite. Geochimica et Cosmochimica Acta 55, 3273-3286.

Saldi, G.D., Jordan, G., Schott, J., Oelkers E.H., 2009. Magnesite growth rates as a function of temperature and saturation state. Geochim. Cosmochim. Acta 73, 5646-5657.

Schiffman, P., Fridleifsson, G.O., 1991. The smectite–chlorite transition in drillhole NJ-15, Nesjavellir geothermal field, Iceland: XRD, BSE and electron microprobe investigations. Journal of Metamorphic Geology 9, 679-696.

Schmidt D.L., Hadley, D.G.,1983 Stratigraphy of the Miocene Baid formation, southern Red Sea coastal plain, Kingdom of Saudi Arabia, USGS Technical Record USGS-TR-04-23, 46 p.

Schmidt D.L., Hadley, D.G., Brown, 1983. Middle tertiary continental rift and evolution of the Red Sea in southwestern Saudi Arabia. USGS Open File report 83-641, 60p.

Schott, J., Pokrovsky, O.S., Oelkers, E.H., 2009. The Link Between Mineral Dissolution/Precipitation Kinetics and Solution Chemistry. Rev. Mineral. Geochemistry 70, 207–258.

Sebai, A., Zumbo, V., Féraud, G., Bertrand, H., Hussain, A. G., Giannérini, G. Campredon, R. (1991). $^{40}Ar/^{39}Ar$ dating of alkaline and tholeiitic magmatism of saudi arabia related to the early red sea rifting. Earth Planet. Sci.Let. 104, 473-487.

Smith. R., 2016. Amorphous Weathering Products: Evidence for Basalt-Water Interactions and the Relevance to Paleo-environments on Mars. A Dissertation Presented in Partial Fulfillment of the Requirements for the Degree Doctor of Philosophy, Arizona State University. 269 p.

Snæbjörnsdóttir, S.Ó., Wiese, F., Fridriksson, T., Ármannsson, H., Einarsson, G. M., Gislason, S. R., 2014. CO_2 storage potential of basaltic rocks in Iceland and the oceanic ridges. Energy Procedia 63, 4585–4600.

Snæbjörnsdóttir S.Ó., Oelkers E.H., Mesfin K., Aradóttir, E.S., Dideriksen, K., Gunnarsson I., Gunnlaugsson, E., Matter J.M., Stute, M. and Gislason, S.R., 2017. The chemistry and saturation states of subsurface fluids during the in situ mineralisation of CO_2 and H_2S at the CarbFix site in SW-Iceland. Int. J. Greenhouse Gas Control 58, 87–102.

Snæbjörnsdóttir, S.Ó., Gislason, S.R., Galeczka, I.M., Oelkers, E.H., 2018a. Reaction path modelling of in-situ mineralisation of CO_2 at the CarbFix site at Hellisheidi, SW-Iceland. Geochimica et Cosmochimica Acta 220, 348-366.

Snæbjörnsdóttir, S.Ó., Tómasdóttir, S., Sigfússon, B., Aradottir, E.S., Gunnarsson, G., Niemi, A., Basirat, F., Dessirier, B., Gislason, S.R., Oelkers, E.H., Franzson, H., 2018b. The geology and hydrology of the CarbFix2 site, SW-Iceland. Energy Procedia 146, 146-157.

Snæbjörnsdóttir, S.Ó., Sigfússon, B., Marieni, C., Goldberg, D., Gislason, S.R., Oelkers, E.H., 2020. Carbon dioxide storage through mineral carbonation. Nature Rev. Earth Env. 1, 90–102.

Sverdrup, H.U., Erlandsson Lampa, M., Beliazid,S., Kurz, D., Axelsson, C., Oelkers, E.H., 2021. The weathering of silicate minerals in soils and watersheds: The parameterization of the weathering kinetics module in the PROFILE and ForSAFE models, an overview.

Tapponnier, P., Dyment, J., Zinger, M.A., Franken, D., Afifi, A.M., Wyllie, A., Ali, H.G., Hanbal, I., 2014. Revisiting seafloor-spreading in the Red Sea: Basement nature, transforms and ocean-continent boundary. AGU Fall meeting 2013 Abstract T12-10. https://ui.adsabs.harvard.edu/abs/2013AGUFM.T12B..04T/abstract

Torres, E., 2020. The Potential for CO_2 Disposal in Western Saudi Arabia: The Jizan Group Basalts. M.S. Thesis, King Abdullah University of Science and Technology, Thuwal, Saudi Arabia, 52 p.

Vahrenkamp, V. and Afif, A. and Tasianas, A. and Hoteit, H., 2021. The Geological Potential of the Arabian Plate for CCS and CCUS - An Overview (April 8, 2021). Proceedings of the 15th Greenhouse Gas Control Technologies Conference 15-18 March 2021,

Voggenreiter, W., Hötzl, H., Jado, A. R., 1988. Red Sea related history of extension and magmatism in the Jizan area (Southwest Saudi Arabia): indication for simple-shear during early Red Sea rifting. Geologische Rundschau 77, 257–274.

Voigt, M., Marieni, C., Clark, D.E., Gíslason, S.R., Oelkers, E.H., 2018a. Evaluation and refinement of thermodynamic databases for mineral carbonation. Energy Procedia 146, 81-91.

Wiese, F., Fridriksson, T. and Ármannsson, H., 2008. CO_2 Fixation by Calcite in High-temperature Geothermal Systems in Iceland. ISOR−2008/003, ÍSOR, Iceland Geosurvey, Reykjavík.

Wurdemann, H., Moller, F., Kuhn, M., Heidug, W.,Christensen, N. P., Born, G., Schilling, F. R. the CO2SINK group. CO2SINK – Feom site characterisaion and risk assessment to monitoring and verification: One year of operational experience with the field laboratory for CO_2 storage at Ketin. Germany. Int. J. Greenhouse Gas Cont., 4, 638-951.

Yang, L., Steefel, C.I., 2008. Kaolinite dissolution and precipitation kinetics at 22 °C and pH 4. Geochim. Cosmochim. Acta 72, 99–116

Yann, R.d.P., Jeffery, M.L., Gutschow, J., Rogelj, J., Christoff, P., Meinshausen, M., 2018. Equitable mitigation to achieve the Paris Agreement goals. Nat. Clim. Change, 7, 38-43

Table 1.
Compositions, formulas, molar volumes and thermal stability field of the secondary phases allowed to precipitate during the reaction path calculations presented in the present study.

Phase	Reaction	Molar volume (cm^3/mol)	Thermal stability	Reference
Carbonates				
Ankerite	$CaFe(CO_3)_2$	66.06		
Aragonite	$CaCO_3$	34.15		
Calcite	$CaCO_3$	36.934		
Magnesite	$MgCO_3$	28.018		
Siderite	$FeCO_3$	29.378		
Fe oxy-hydroxides				
Goethite	FeOOH	20.82		
Hematite	Fe_2O_3	30.274		
Ilmenite	$FeTiO_3$	32.15		
Magnetite	Fe_3O_4	44.524		
Titanite	$CaTiSiO_5$	55.65		
Feldspars				
Albite	$NaAlSi_3O_8$	100.25	≥250 °C	[1]
K-feldspar	$KAlSi_3O_8$	108.87	≥250 °C	[1]
Clay minerals				
Saponite-Fe-Fe	$Fe_{3.175}Al_{0.35}Si_{3.65}O_{10}(OH)_2$	142.672	<200 °C	[2, 3, 4, 5]
Saponite-Fe-K	$K_{0.35}Fe_3Al_{0.35}Si_{3.65}O_{10}(OH)_2$	147.639	<200 °C	[2, 3, 4, 5]
Saponite-Mg-Mg	$Mg_{3.175}Al_{0.35}Si_{3.65}O_{10}(OH)_2$	140.285	<200 °C	[2, 3, 4, 5]
Saponite-Mg-K	$K_{0.35}Mg_3Al_{0.35}Si_{3.65}O_{10}(OH)_2$	145.383	<200 °C	[2, 3, 4, 5]
Saponite-Mg-Fe	$Fe_{0.175}Mg_3Al_{0.35}Si_{3.65}O_{10}(OH)_2$	140.416	<200 °C	[2, 3, 4, 5]
Beidellite-Ca	$Ca_{0.175}Al_{2.35}Si_{3.65}O_{10}(OH)_2$	133.081	<200 °C	[2, 3, 4, 5]
Beidellite-Fe	$Fe_{0.175}Al_{2.35}Si_{3.65}O_{10}(OH)_2$	134.293	<200 °C	[2, 3, 4, 5]
Beidellite-K	$K_{0.35}Al_{2.35}Si_{3.65}O_{10}(OH)_2$	137.214	<200 °C	[2, 3, 4, 5]
Beidellite-Mg	$Mg_{0.175}Al_{2.35}Si_{3.65}O_{10}(OH)_2$	132.116	<200 °C	[2, 3, 4, 5]
Beidellite-Na	$Na_{0.35}Al_{2.35}Si_{3.65}O_{10}(OH)_2$	134.522	<200 °C	[2, 3, 4, 5]
Mica				
Celadonite	$KMgAlSi_4O_{10}(OH)_2$	157.1	≤100 °C	[2]
Chlorites				
Clinochlore	$Mg_5Al_2Si_3O_{10}(OH)_8$	207.11	>200 °C	[2, 4, 5]
Zeolites				
Analcime	$Na_{0.96}Al_{0.96}Si_{2.04}O_6{:}H_2O$	97.43	<200 °C	[1]
Chabazite-Ca	$CaAl_2Si_4O_{12}{:}6H_2O$	247.45	≤100 °C	[3]
Chabazite-Na	$Na_2Al_2Si_4O_{12}{:}6H_2O$	247.45	≤100 °C	[3]
Laumontite	$CaAl_2Si_4O_{12}{:}4.5H_2O$	209.68	100-200 °C	[3]
Mordenite-Ca	$Ca_{0.5}AlSi_5O_{12}{:}4H_2O$	208.74	<230 °C	[6]
Stilbite-Ca	$CaAl_2Si_7O_{18}{:}7H_2O$	333.48	70-150 °C	[6]
Thomsonite	$Ca_2NaAl_5Si_5O_{20}{:}6H_2O$	338.10	≤100 °C	[4]
Wairakite	$CaAl_2Si_4O_{12}{:}2H_2O$	190.35	>180 °C	[1, 3]
Other silicates				
Epidote	$Ca_2FeAl_2Si3O_{12}OH$	139.2	>200 °C	[1, 7]
Kaolinite *	$Al_2Si_2O_5(OH)_4$	99.52		
Quartz	SiO_2	22.68	>180 °C	[4]
Chalcedony	SiO_2		75-180 °C	[9]
Amorphous silica **	SiO_2	29.00	25-75 °C	[9]
Prehnite	$Ca_2Al_2Si_3O_{10}(OH)_2$	140.33	>200 °C	[7]

[1] Larsson et al. (2002), [2] Alt (1995), [3] Kristmannsdóttir (1979), [4] Snæbjörnsdóttir et al. (2018b), [5] Schiffman and Fridleifsson (1991), [6] Krìstmannsdóttir and Tomasson (1978), [7] Rose (1991), [8] Gysi and Stefánsson (2012 [9] Neuhoff et al. (2000).

Table 2
A summary of the relative mineral volume percentages in basaltic rock samples as determined by X-ray diffractometry. The rock samples used for the reactivity experiments are highlighted.

Sample	Plag	Aug	Qtz	Amph	Ttn	Cham	Or	Mt	Ep	Other
Volcanics										
AND 03	64.5[1]	-	0.7	-	15.9	9.2	-	-	-	Hm (7.4)
WDP 01	46.0[1]	-	13.1	-	6.6	5.6	16.1	-	4.2	Mghm (8.4)
WDP 05	54.5[1]	-	6.7	-	1.9	26.5	10.5	-	-	Hm (0.3)
WJB 03	42.0[1]	6.9	21.0	5.8[5]	5.3	10.2	-	-	4.4	Prhn (4.4)
WJU 01	59.0[1]	2.8	12.3	1.2[5]	22.8	2.0	-	-	-	-
JG 202	55.1[1]	-	4.6	-	13.7	7.3	-	-	17.8	Hm (1.5)
Dikes										
AND 02	61.0[2]	25.7	8.2	-	-	3.5	-	-	-	Tmt (3.5)
WDH 01	64.0[4]	15.1	3.5	1.8[5]	3.9	7.8	-	-	-	Analc (1.5), Cal (1.5), Tmt (0.9)
WJS 02	59.2[1]	20.2	-	1.9[5]	7.7	9.7		1.3	-	-
WJU 03	49.3[4]	18.0	-	9.1[7]	4.1	9.8	3.3	-	6.5	-
JG 101	48.1[1]	20.3	7.3	6.2[5]	6.1	5.9	5.1	1.1	-	-
JG 103	48.2[1]	7.4	-	15.7[5]	5.2	6.6	11.1	-	5.8	-
JG 105	59.7[2]	27.0	-	5.1[6]	-	0.7	1.6	3.9	-	Cal (1.1), Ilm (0.8)
JG 203	47.8[4]	20.3	-	8.0[7]	-	10.0	-	-	5.8	Epist (7.3), Py (0.7)

The abbreviations, Plag, Aug, Amph, Analc, Cal, Cham, Dsp, Ep, Epist, Hm, Iml, Liz, Mt, Or, Prhn, Py, and Tmt, refer to plagioclase, augite, amphibole, analcime, calcite, chamosite, diaspore, epidote, epistilbite, hematite, ilmenite, lizardite, magnetite, orthoclase, prehnite, pyrite and titanomagnetite, respectively.

1) Reported as Albite
2) Reported as Andesine
3) Reported as Oligioclase
4) Reported as Labradorite
5) Reported as Actinolite
6) Reported as Cummingtonite
7) Reported as Horneblende

Table 3
Major chemical compositions of the Jizan basaltic rocks, reported as oxide percent determined by X-ray fluorescence (XRF) analyses. The rock samples used for the reactivity experiments are highlighted.

Sample	SiO_2	Al_2O_3	Fe_2O_3	CaO	Na_2O	MgO	TiO_2	K_2O	P_2O_5	MnO	LOI[1]
Volcanics											
AND 03	40.7	18.0	13.4	5.4	5.2	9.3	2.0	0.12	0.26	0.17	5.0
WDP 01	45.6	14.5	14.1	6.6	5.7	3.6	2.6	< 0.1	0.44	0.15	4.8
WDP 05	52.6	15.8	10.4	3.5	7.1	2.7	2.2	1.3	0.85	0.11	2.9
WJB 03	51.1	13.2	12.4	6.1	4.5	4.7	2.1	0.79	0.32	0.20	3.3
WJU 01	50.7	13.1	12.8	5.1	4.1	5.0	2.4	0.98	0.34	0.22	4.3
JG 202	43.5	17.6	10.7	11.2	3.7	8.1	1.8	0.26	0.32	0.16	2.1
Dikes											
AND 02	43.7	14.8	11.4	9.7	4.6	7.2	1.2	0.09	0.18	0.18	6.4
WDH 01	45.7	21.2	10.2	11.0	4.6	3.7	2.0	0.61	0.32	0.15	<0.1
WJS 02	45.0	15.0	15.1	6.0	6.5	5.2	2.5	0.84	0.36	0.22	2.7
WJU 03	43.2	15.4	15.6	8.0	5.6	4.3	2.3	1.1	0.41	0.26	3.1
JG 101	47.2	15.1	14.3	8.3	5.6	3.9	2.2	0.99	0.28	0.21	1.8
JG 103	44.9	13.9	15.5	8.1	5.2	4.7	2.5	0.76	0.42	0.25	3.3
JG 105	42.2	16.0	13.4	9.9	5.3	5.8	3.2	0.52	0.32	0.20	2.4
JG 203	46.8	15.8	13.3	7.5	5.6	3.8	2.4	0.71	0.59	0.20	2.9

1) *Loss on Ignition*

Table 4
Summary of the experimentally measured Si release rates from selected Jizan area rocks and corresponding rate parameters for Eqn. (1).

Sample	k (mol/m^2/s)	n	Log (r/(mol/m^2/s)) at pH=4	Log (r/(mol/m^2/s)) at pH=6
JG202 a	1.51×10^{-5}	-1.0	-8.82	-10.82
JG 202 b	6.34×10^{-6}	-0.95	-8.99	-10.89
JG 202 c	7.54×10^{-6}	-1	-9.12	-11.12
WJS 02a	3.79×10^{-8}	-0.45	-9.16	-10.16
WJS 02 c	1.81×10^{-8}	-0.40	-9.34	-10.14
WJU 01	2.68×10^{-7}	-0.60	-8.94	-10.14
WJU 03	1.81×10^{-7}	-0.60	-9.14	-10.34

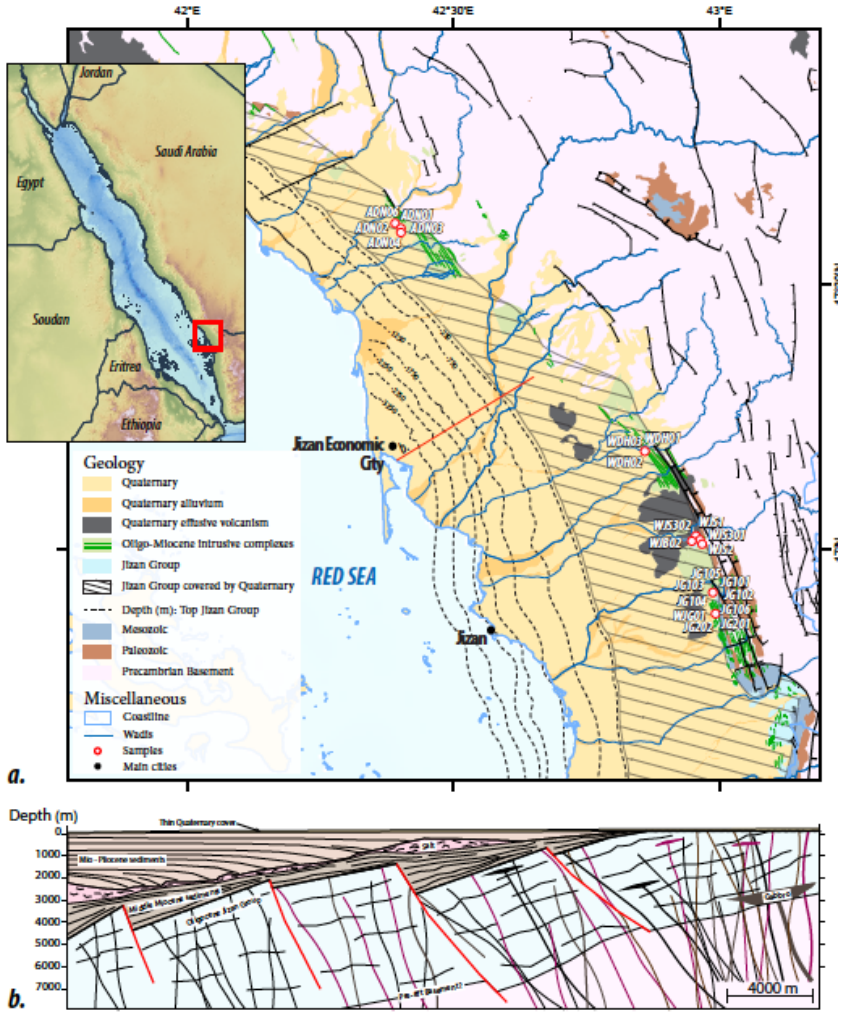

Figure 1a, b. Top: a) A simplified geologic map of the southwest coast of Saudi Arabia. Rock sampling locations are shown by red symbols. Bottom, b) a simplified geologic cross section from east to west from the Red Sea. The width of the cross section is approximately 30 km.

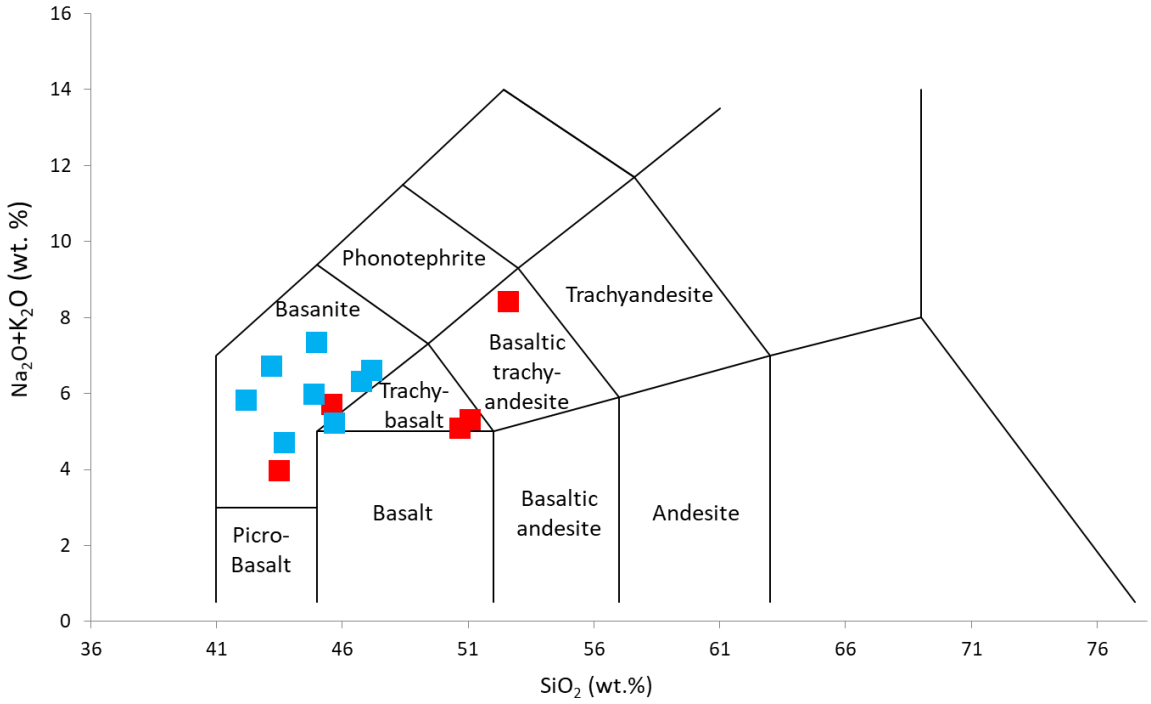

Figure 2. Total Akali-Silica (TAS) classification diagram (Le Bas et al. 1986) for the volcanic (red) and subvolcanic/dike (blue) basaltic rocks from the Jizan region.

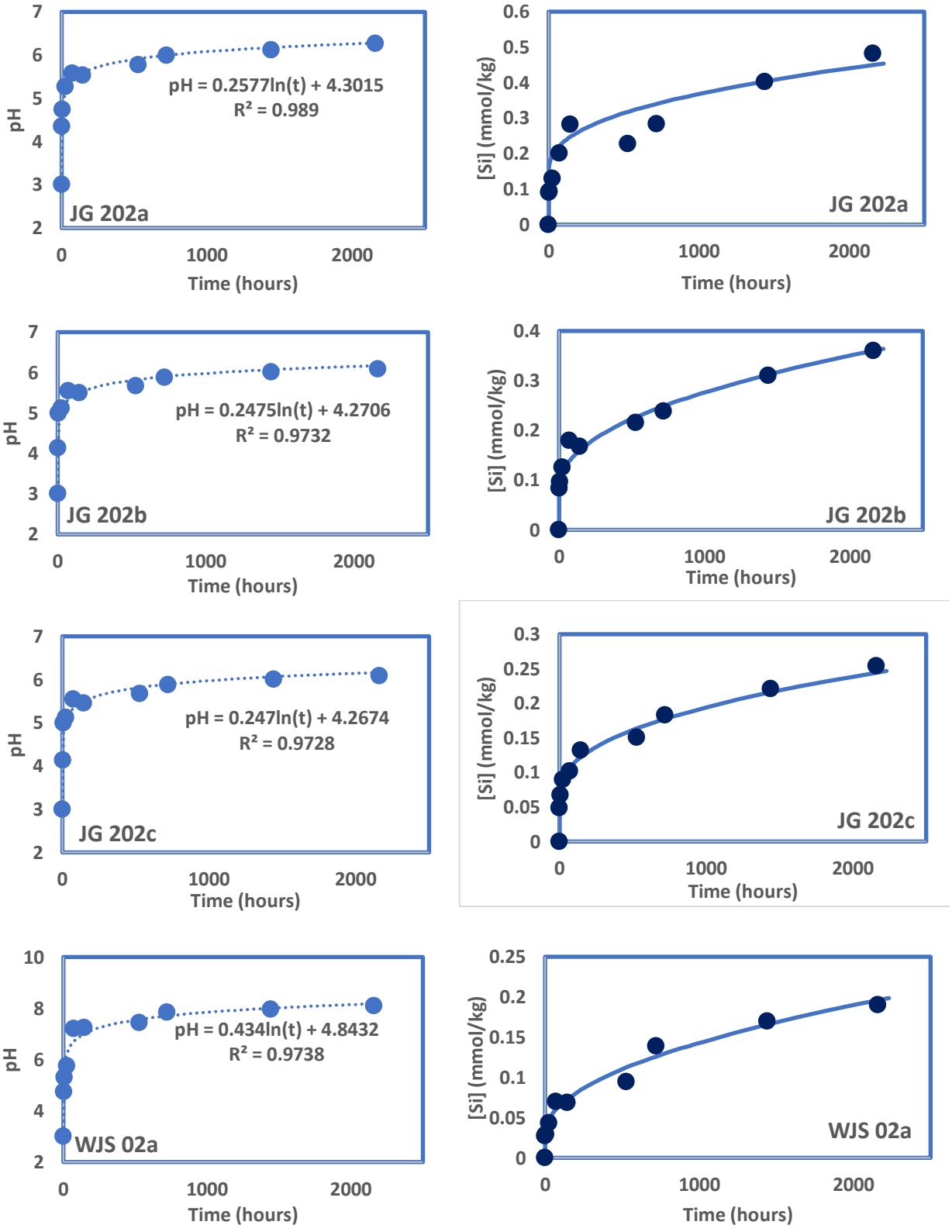

Figure 3 (part 1).

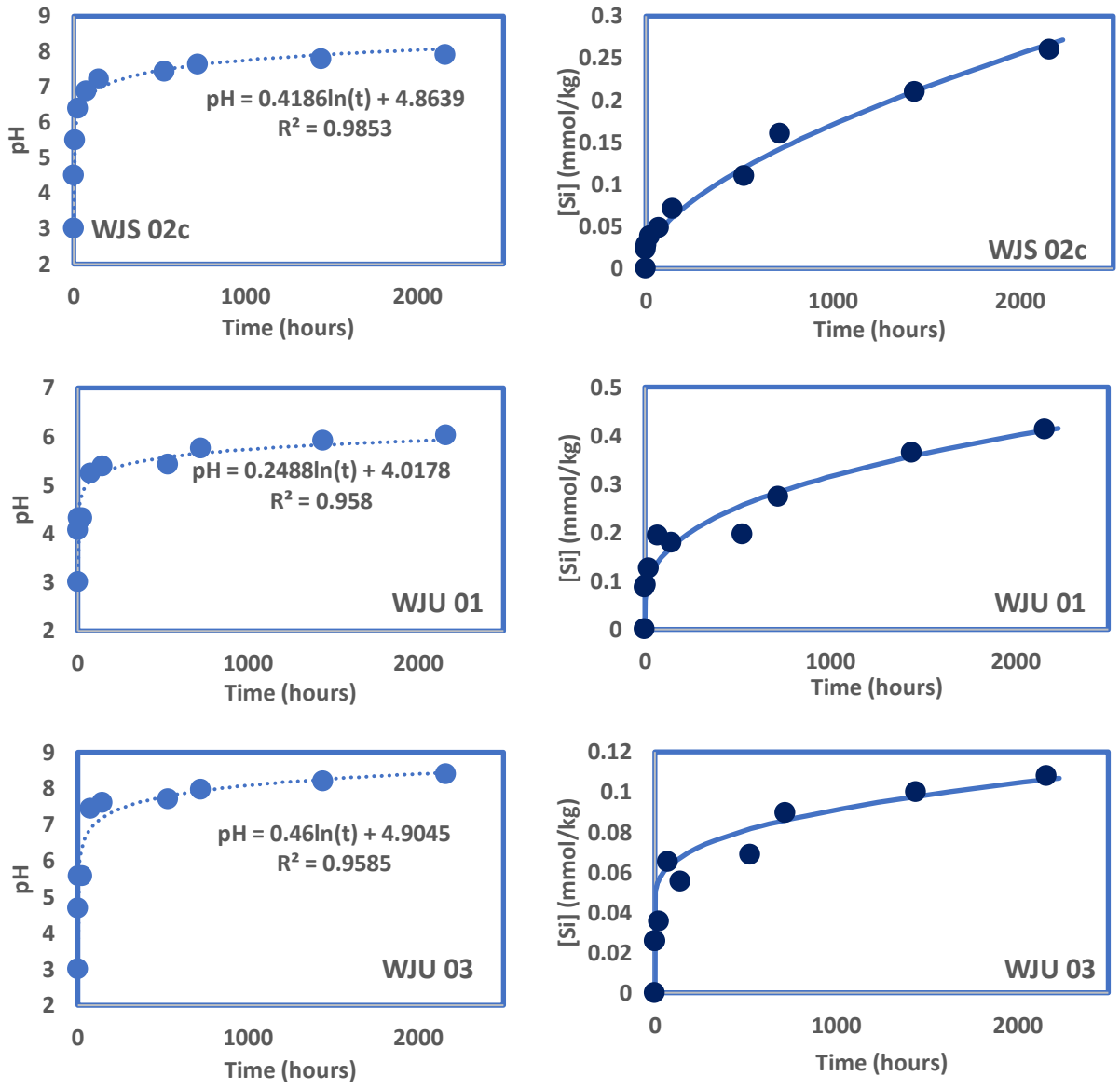

Figure 3 (part 2). Temporal variation of reactive pH and Si concentration in all experiments. The symbols represent measured values. The curves in the pH plots correspond to a least squares fit of the measured values, with the resulting fit equation and goodness of fit parameter provided. The curves in the Si concentration plots present a fit of these data to Eqn. (1) using the corresponding temporal pH equation provided in the Figure.

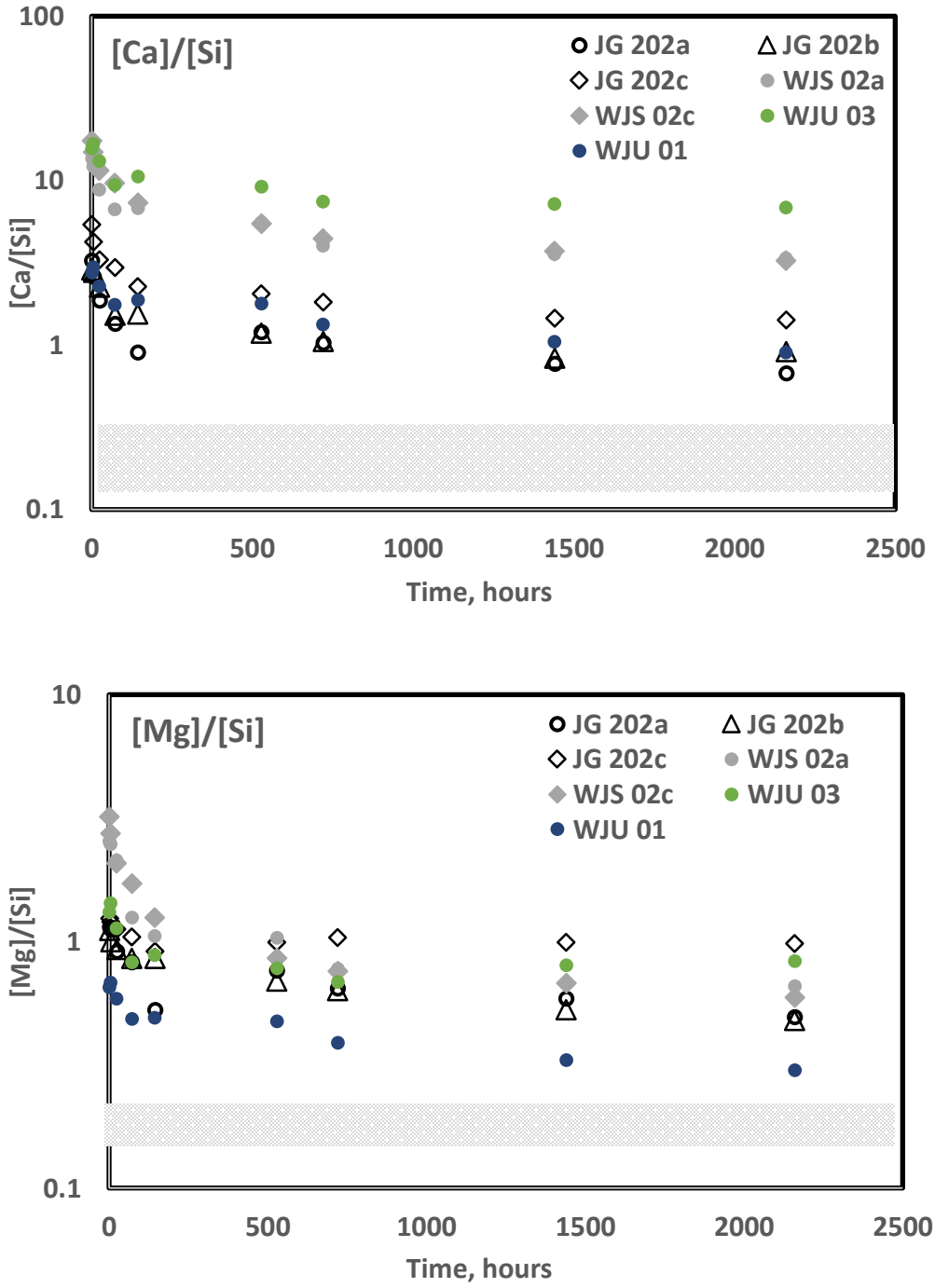

Figure 4. a) The molar Ca to Si ratio and b) the molar Mg to Si ratio of the fluids sampled during all experiments as a function of time. The grey rectangles indicate the corresponding molar elemental ratios of the dissolving solids in the experiments. The identity of each experiment is noted by the symbol as defined in the figure.

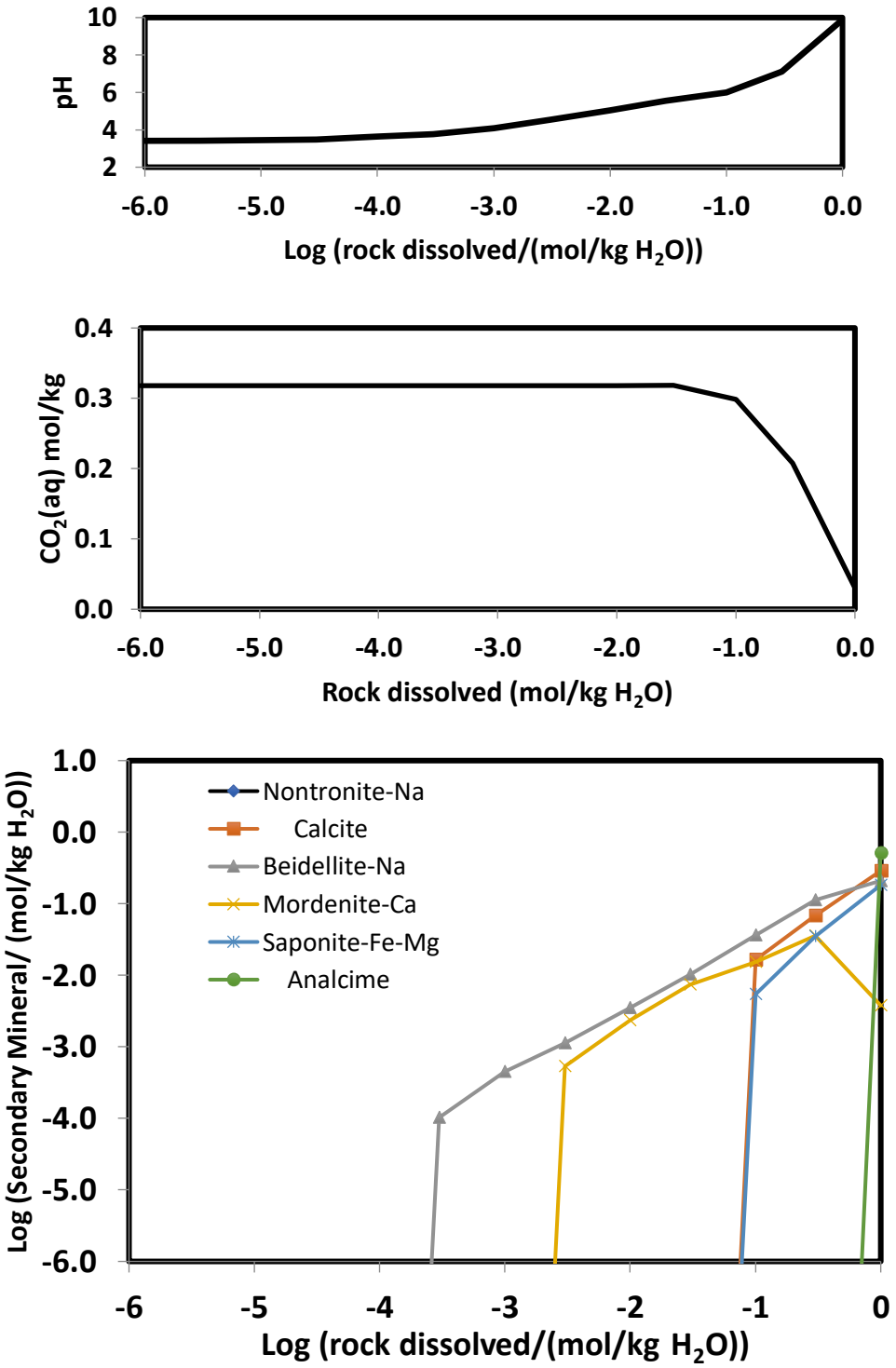

Figure 5. Results of reaction path calculations for a representative altered Jizan basalt reacted with an aqueous 0.1 M NaCl solution charged with initially 10 bar of CO_2 pressure as a function of the mass of rock dissolved at 25 ^{o}C. Top: pH; middle: Dissolved inorganic carbon; bottom; secondary minerals formed

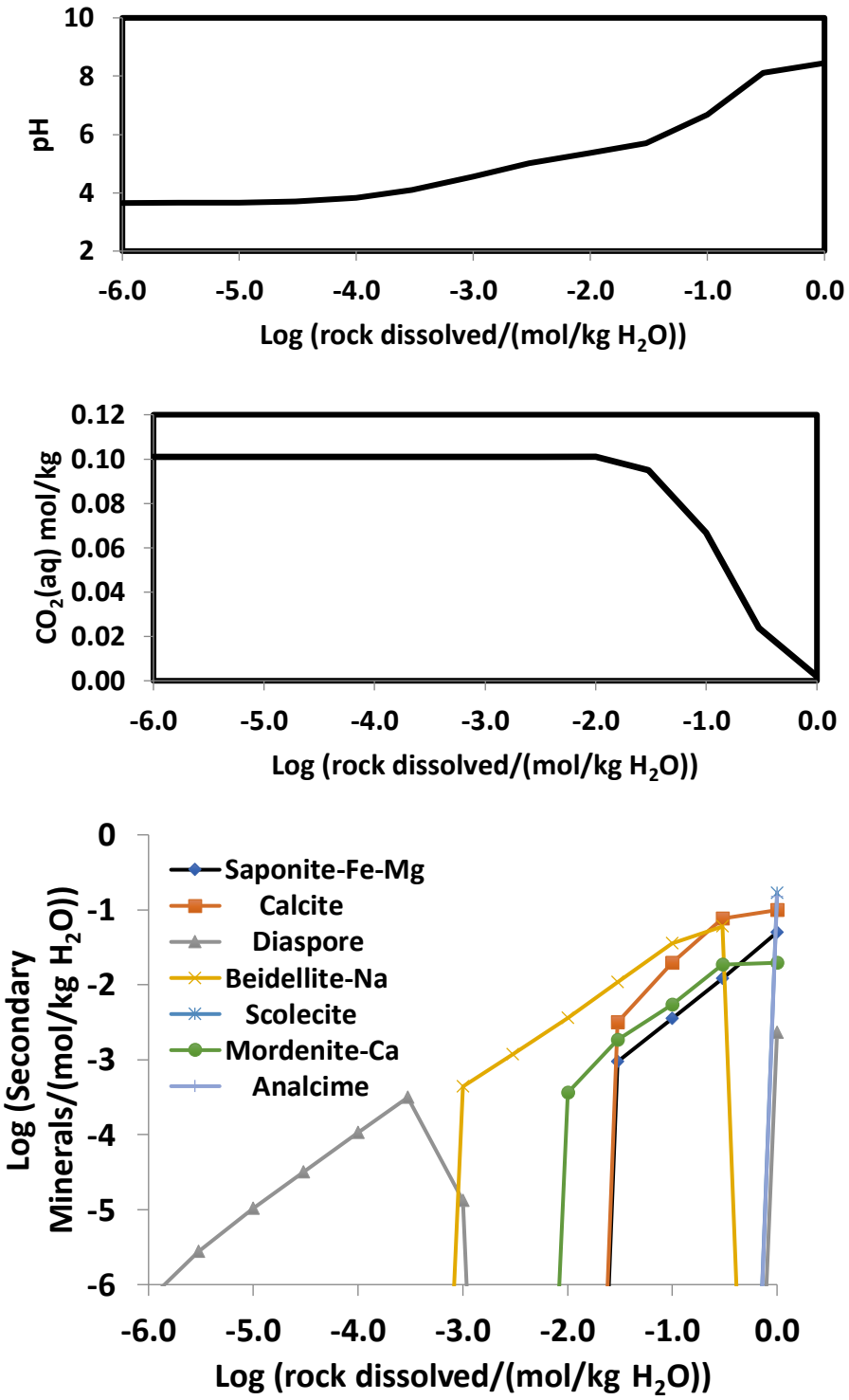

Figure 6. Results of reaction path calculations for a representative altered Jizan basalt reacted with an aqueous 0.1 M NaCl solution charged with initially 10 bar of CO_2 pressure as a function of the mass of Jizan rock dissolved. Top: pH; middle: Dissolved inorganic carbon; bottom; secondary minerals formed.

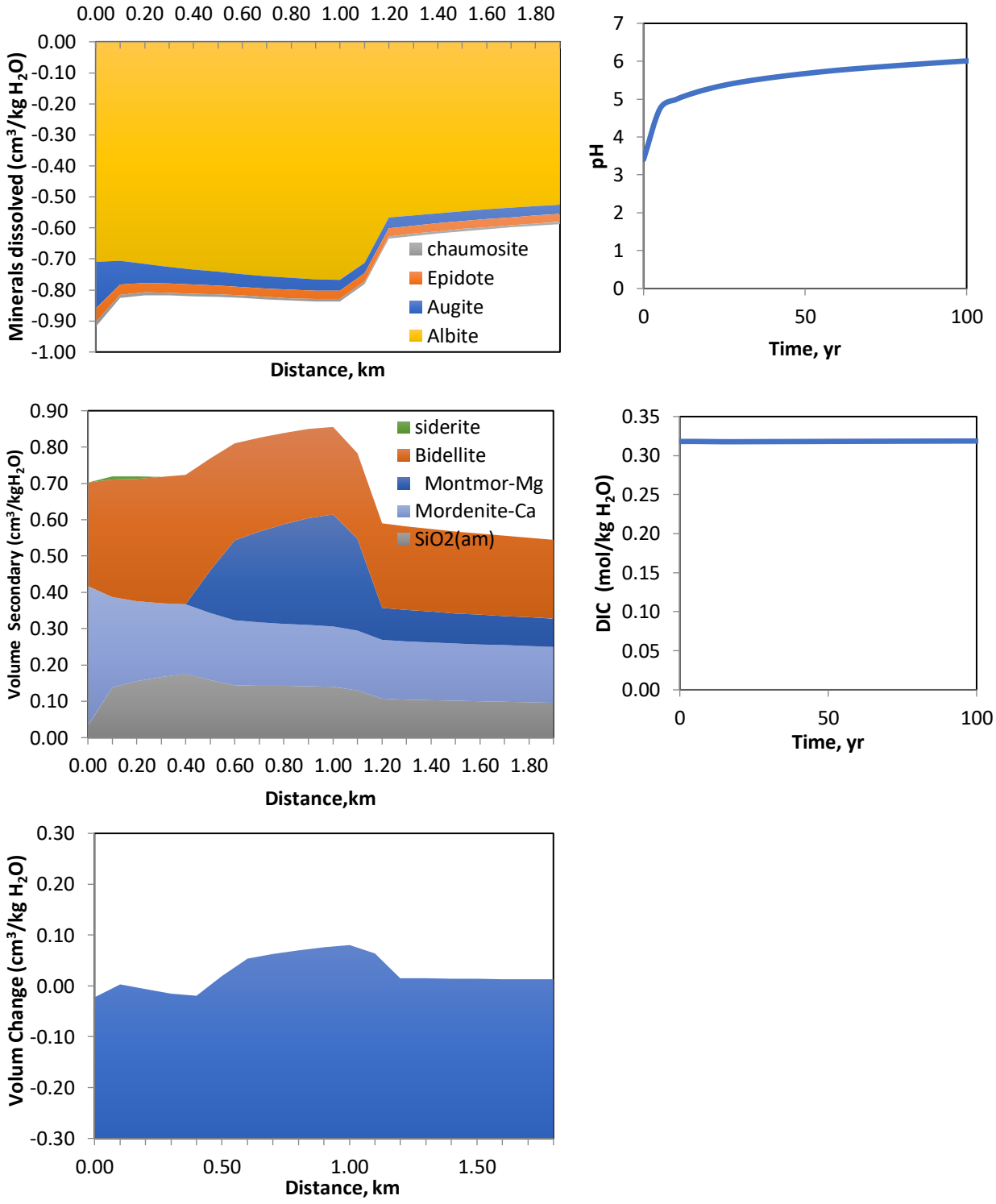

Figure 7. a) Volume of minerals dissolved, b) precipitated c) net volume change per 100 meter distance in a 1mm fracture in response to the injection of a 0.1 m NaCl solution initially charged with 10 bar CO_2 into a representative altered Jizan basalt at 25 °C d) the pH and e) the total dissolved inorganic carbon in the fluid phase over time as it moves 2 km along the fracture over 100 years.

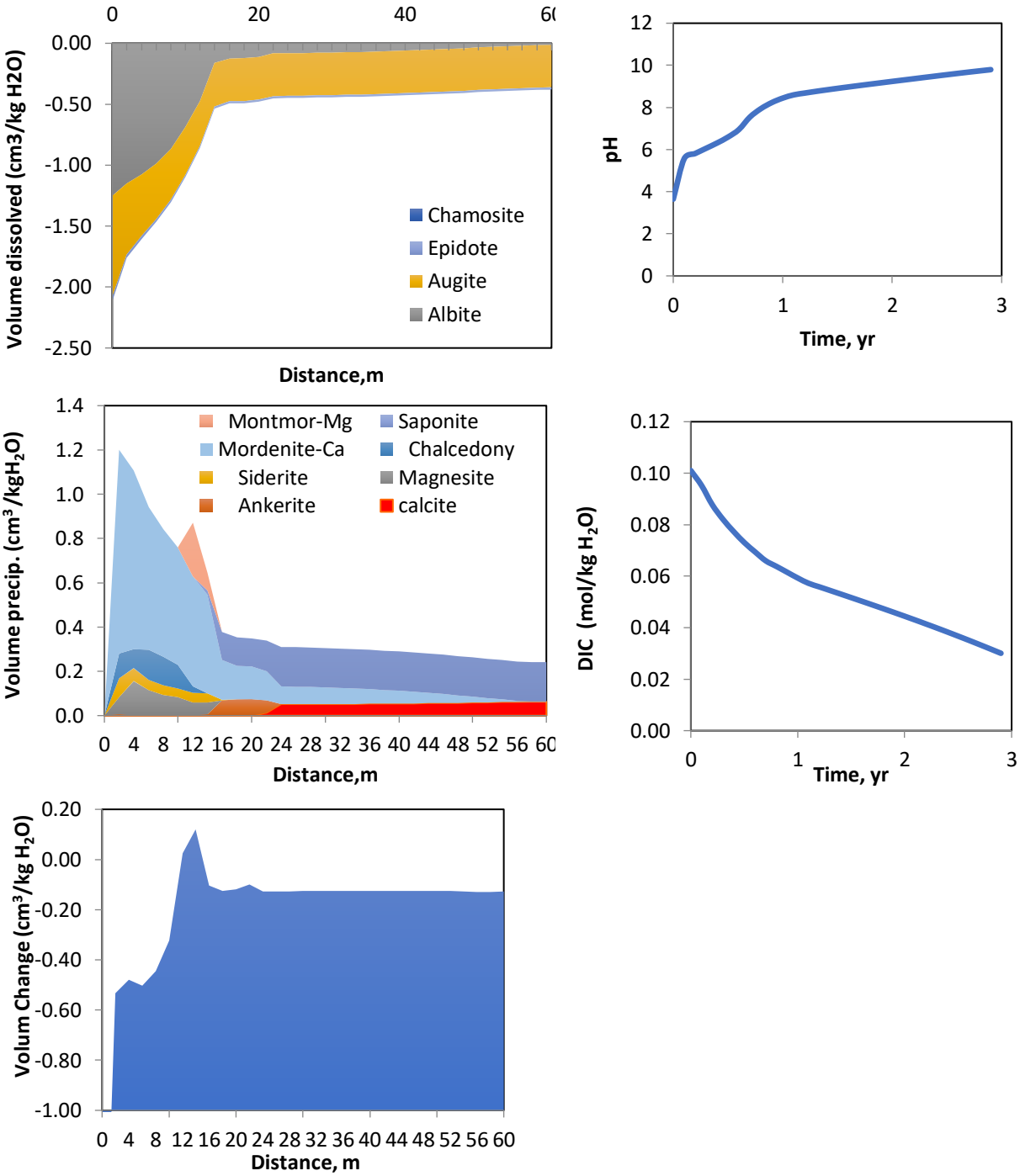

Figure 8. a) Volume of minerals dissolved, b) precipitated c) net volume change per 20 meter distance in a 1mm fracture in response to the injection of a 0.1 m NaCl solution initially charged with 10 bar CO_2 into a representative altered Jizan basalt at a temperature of 100 °C. d) the pH and e) the total dissolved inorganic carbon in the fluid phase over time as it moves 20 m along the fracture over 1 year.